An *A Posteriori* Error Reduction Scheme for the Three-Dimensional Finite Element Solution of Maxwell's Equations

Ümit Pekel, and Robert Lee, *Member, IEEE*

***Abstract*— The accuracy of the finite element method (FEM) depends on the properties of the mesh which covers the problem geometry. The accuracy can usually be improved by increasing the element density in the mesh or the order of the shape functions in the elements at the expense of a significant increase in computation time. Instead, in this paper an *a posteriori* error reduction scheme is applied to improve the accuracy in the solution of three-dimensional electromagnetic boundary value problems. In this scheme, first the FEM solution is generated by the use of lower-order shape functions. Then the numerical error is expressed in terms of higher-order shape functions and calculated on an element-by-element basis from information derived from the FEM solution. Finally, this error is added to the FEM solution to improve its accuracy. The degree of error reduction which is achieved with the application of this scheme is demonstrated by means of several simple electromagnetic boundary value problems.**

I. Introduction

THE ACCURACY of the finite element method (FEM) depends upon the gridding scheme used to mesh the geometry. The solution becomes more accurate when either the mesh becomes finer or the order of the shape function is increased, but in exchange there is a corresponding increase in computation time. For the user it is important to find the optimum mesh density which produces both an accurate and efficient solution. One area of research that is very active is adaptive mesh refinement methods [1]–[5]. In these methods, the problem is solved multiple times where after each solution, mesh refinement is carried out in selective regions of the mesh. The selective regions are chosen from an *a posteriori* analysis of the previous solution to determine the regions of the mesh with the greatest error. In this way, one can increase the mesh density or the order of the shape functions only in those regions where a large error is predicted. Thus, the discretization of an arbitrary geometry is automatically done to some error criterion that the user specifies.

The ideas in adaptive mesh refinement can also be used to improve the FEM solution without having to recompute a global matrix solution. Kelly [6] used a posteriori information to find an improved solution which minimizes the global energy norm of the error and at the same time satisfies certain physical laws. The solution is computed in an element-by-element manner so that the computation time of the improved solution is small compared to the one of the original solution. He applies his method to Laplace's equation in one and two dimensions.

Using Kelly's work as a basis, Ohtsubo and Kitamura [7] developed another error reduction scheme for two-dimensional elastic problems. In this scheme, they generated finite element equations for the error in terms of the a posteriori information. They then decoupled the finite element equations so that the elements are independent of one another by enforcing several physical constraints on the solution. The resulting error was added back into the original solution to create an improved solution.

In this paper, we are extending the work of Ohtsubo and Kitamura to solve three-dimensional electromagnetic wave problems. In our analysis, we plan to express the error in terms of two *a posteriori* parameters. The first parameter is an error residual which is generated from the fact that the numerical solution does not satisfy the wave equation. The second parameter measures the discontinuity of the tangential fields at inter-element surfaces in the numerical solution. We can compute an error from these two parameters by following a systematic procedure similar to [7]. To validate this method, several simple rectangular waveguide geometries are considered.

II. Formulation

Let us consider a volumetric, source-free region of space denoted by Ω, where Ω can be divided into finite elements Ω_m (Fig. 1). From Maxwell's equations, we can show that the electric field satisfies the differential equation

$$\nabla \times \left(\frac{1}{j\omega\mu} \nabla \times \vec{E} \right) + j\omega\epsilon^* \vec{E} = 0 \qquad (x, y, z) \in \Omega \quad (1)$$

where the $\exp(j\omega t)$ time harmonic variation has been suppressed and $\epsilon^* = \epsilon - j\sigma/\omega$. The finite element discretization of the associated variational expression for (1) is known to produce spurious solutions. However, an alternative differential equation based on the vector Helmholtz equation has been used to produce non-spurious solutions [8]. The differential equation is given by

$$\nabla \times \left(\frac{1}{j\omega\mu} \nabla \times \vec{E} \right) + j\omega\epsilon^* \vec{E} - \nabla \left(\frac{1}{j\omega\mu\epsilon^*} \nabla \cdot (\epsilon^* \vec{E}) \right) = 0 \qquad (x, y, z) \in \Omega \quad (2)$$

Manuscript received October 23, 1992; revised May 20, 1994. This work was sponsored by NSF Grant ECS-9111266 and the Joint Services Electronics Program under Contract N00014-89-J-1007.

The authors are with the ElectroScience Laboratory, Department of Electrical Engineering, The Ohio State University, Columbus, Ohio 43212 USA.

IEEE Log Number 9407278.

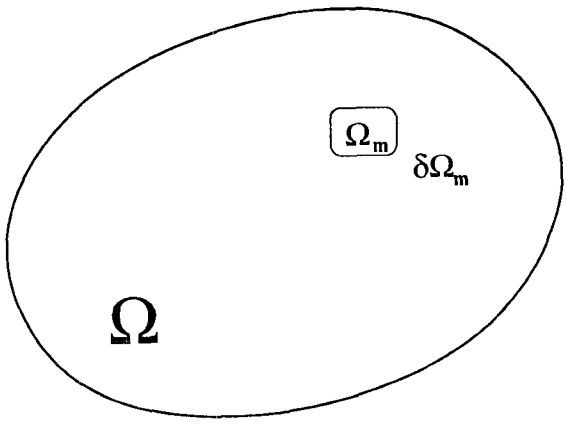

Fig. 1. Problem geometry.

The corresponding variational expression over the entire grid is

$$\sum_m \iiint_{\Omega_m} \frac{1}{j\omega\mu}(\nabla\times\vec{E})\cdot(\nabla\times\vec{\phi}_i) + j\omega\epsilon^*\vec{E}\cdot\vec{\phi}_i + \frac{1}{j\omega\mu\epsilon^*}\nabla\cdot(\epsilon^*\vec{E})(\nabla\cdot\vec{\phi}_i)\,dv = \sum_m \iint_{\partial\Omega_m} \frac{1}{j\omega\mu\epsilon^*}\nabla\cdot(\epsilon\vec{E})\vec{\phi}_i\cdot\hat{n} + (\hat{n}\times\vec{H})\cdot\vec{\phi}_i\,dS \tag{3}$$

where $\partial\Omega_m$ is the surface enclosing element m. The continuity of tangential $\vec{E}$ and normal $\vec{D}$ is enforced directly at the nodes. Assuming that there are no surface currents or charges at the inter-element boundaries, the surface integral in (3) vanishes everywhere except at the boundary of the mesh.

We can now choose a set of shape functions to approximate the electric field and generate a numerical solution using FEM. Unfortunately, because the shape functions are only finite order polynomials with C^0 continuity (Function is continuous, but first derivative is discontinuous.), it produces a numerical solution which only approximates the real solution. Let the finite element approximation for the electric field be denoted by $\tilde{E}$. Then $\tilde{E}$ (in element Ω_m) satisfies the equation,

$$\nabla\times\left(\frac{1}{j\omega\mu}\nabla\times\tilde{E}\right) + j\omega\epsilon^*\tilde{E} - \nabla\left(\frac{1}{j\omega\mu\epsilon^*}\nabla\cdot(\epsilon^*\tilde{E})\right) = \vec{r}_m \quad (x, y, z)\in\Omega_m \tag{4}$$

where $\vec{r}_m$ is the residual due to the error in the FEM solution. A weak form of (4), which is valid over the entire grid, is

$$\sum_m \iiint_{\Omega_m} \frac{1}{j\omega\mu}(\nabla\times\tilde{E})\cdot(\nabla\times\vec{\phi}_i) + j\omega\epsilon^*\tilde{E}\cdot\vec{\phi}_i + \frac{1}{j\omega\mu\epsilon^*}\nabla\cdot(\epsilon^*\tilde{E})(\nabla\cdot\vec{\phi}_i) - (\vec{r}_m\cdot\vec{\phi}_i)\,dv = \sum_m \iint_{\partial\Omega_m} \frac{1}{j\omega\mu\epsilon^*}\nabla\cdot(\epsilon\tilde{E})(\vec{\phi}_i\cdot\hat{n}) + (\hat{n}\times\tilde{H})\cdot\vec{\phi}_i\,dS \tag{5}$$

where $\tilde{H}$ is the numerical solution for the magnetic field and is given by

$$\nabla\times\tilde{E} = -j\omega\mu\tilde{H} \tag{6}$$

Unlike the exact magnetic field in (3), $\tilde{H}$ is discontinuous at inter-element boundaries, thereby generating fictitious surface currents between the elements. In addition, a fictitious charge, which is given by $\nabla\cdot\epsilon\tilde{E}$, may be present at the inter-element boundary.

By summing over all the elements in the grid, we obtain the following equation from (5):

$$\iiint_{\Omega} \frac{1}{j\omega\mu}(\nabla\times\tilde{E})\cdot(\nabla\times\vec{\phi}_i) + j\omega\epsilon^*\tilde{E}\cdot\vec{\phi}_i + \frac{1}{j\omega\mu\epsilon^*}\nabla\cdot(\epsilon^*\tilde{E})(\nabla\cdot\vec{\phi}_i) - (\vec{r}\cdot\vec{\phi}_i)\,dv = \sum_{m,k}\iint_{\partial\Omega_{mk}} \vec{\rho}_{mk}\cdot\vec{\phi}_i\,dS \tag{7}$$

where $\partial\Omega_{mk}$ is the surface joining elements m and k. Note that the residual $\vec{r}$ has no subscript since it is associated with the entire mesh rather than a single element in the mesh. In (7), we have excluded the term associated with the boundary conditions on the mesh. This term will be considered later.

The sum on the right hand side of (7) is evaluated over all the inter-element boundary surfaces in the mesh. The term $\vec{\rho}_{mk}$, which represents the fictitious currents and charges at the inter-element boundaries, is given by

$$\vec{\rho}_{mk} = \frac{1}{j\omega\epsilon_m\mu_m}\nabla\cdot(\epsilon_m\tilde{E}_m)\hat{n}_m + \hat{n}_m\times\tilde{H}_m - \frac{1}{j\omega\epsilon_k\mu_k}\nabla\cdot(\epsilon_k\tilde{E}_k)\hat{n}_k - \hat{n}_k\times\tilde{H}_k \tag{8}$$

The subscripts, m and k, on the right hand side of the equation indicate the element in which the vector quantities and material parameters are evaluated.

In this paper, we seek to obtain an estimate for the error in the finite element solution. It is obvious from the previous equations that the non-zero values of $\vec{r}$ and $\vec{\rho}_{mk}$ are due to the errors in the numerical solution; therefore, an equation for the error can be written in terms of these two variables. The error $\vec{e}$ due to the finite element approximation is defined to be

$$\vec{e} = \vec{E} - \tilde{E} \tag{9}$$

An expression for this error can be found by subtracting (7) from (3) to obtain

$$\iiint_{\Omega} \frac{1}{j\omega\mu}(\nabla\times\vec{e})\cdot(\nabla\times\vec{\phi}_i) + j\omega\epsilon^*\vec{e}\cdot\vec{\phi}_i + \frac{1}{j\omega\mu\epsilon^*}\nabla\cdot(\epsilon^*\vec{e})(\nabla\cdot\vec{\phi}_i) - (\vec{r}\cdot\vec{\phi}_i)\,dv = \sum_{m,k}\iint_{\partial\Omega_{mk}} \vec{\rho}_{mk}\cdot\vec{\phi}_i\,dS \tag{10}$$

The terms, $\vec{r}$ and $\vec{\rho}_{mk}$, are known a posteriori from the original FEM solution for the electric fields. Thus, we can solve for the error by applying FEM to (10). The same shape functions that are used to approximate the fields in (5) can also be used to approximate the error in (10). However, it has been found [6] that the dominant term in the error is associated with the polynomials which are one order higher than those used to approximate the fields. Therefore, a higher order

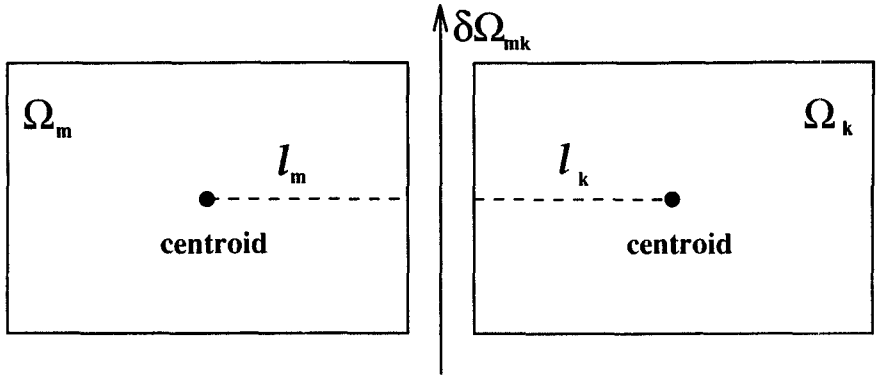

Fig. 2. A side view of elements Ω_m and Ω_k is shown. The length l_m is traced from the centroid of element Ω_m to the centroid of surface $\partial\Omega_{mk}$. Likewise, l_k is traced from the centroid of element Ω_k to the centroid of surface $\partial\Omega_{mk}$.

shape function is used to approximate the error. In our case, we use an 8-node isoparametric hexahedron to represent the fields and a 20-node isoparametric hexahedron to represent the error. The solution of (10) with 20-node hexahedra is computationally expensive because the term $\vec{\rho}_{mk}$ couples the finite element equations between adjacent elements. In fact, the error computation would require as much time as the field calculation in which 20-node hexahedra are used as the shape functions. Based on this observation, a direct solution of (10) is not efficient for estimating the error in the FEM solution.

In order to make the error calculation efficient, the error in each element must be decoupled from the other elements. To accomplish this decoupling, we must remove the constraint that the fields be continuous at the nodes. In addition, the variable $\vec{\rho}_{mk}$ must be decomposed into two independent terms, $\vec{\rho}_m$ and $\vec{\rho}_k$, where the first term is associated with the mth element and the second is associated with the kth element. The resulting equation for the error in element Ω_m is

$$\iiint_{\Omega_m} \frac{1}{j\omega\mu}(\nabla\times\vec{e})\cdot(\nabla\times\vec{\phi}_i) + j\omega\epsilon^*\vec{e}\cdot\vec{\phi}_i + \frac{1}{j\omega\mu\epsilon^*}\nabla\cdot(\epsilon^*\vec{e})(\nabla\cdot\vec{\phi}_i) - (\vec{r}_m\cdot\vec{\phi}_i)\,dv = \iint_{\partial\Omega_m}\vec{\rho}_m\cdot\vec{\phi}_i\,dS \tag{11}$$

Since the elements are decoupled, the error in each element is found by solving an $N_e \times N_e$ matrix equation (from (11)) where N_e is the number of unknowns associated with the element. For the 20-node hexahedron, $N_e = 60$.

The manner in which we divide $\vec{\rho}_{mk}$ into $\vec{\rho}_m$ and $\vec{\rho}_k$ is important in determining how accurately the error is approximated. Unfortunately, there does not seem to be a way to split $\vec{\rho}_{mk}$ such that the accuracy of the error is optimized. In our case, we choose a simple splitting scheme proposed by Ohtsubo and Kitamura [7]. The division is based on the relative sizes of neighboring elements and is given by

$$\vec{\rho}_m = \frac{l_m}{l_m + l_k}\vec{\rho}_{mk}; \quad \vec{\rho}_k = \frac{l_k}{l_m + l_k}\vec{\rho}_{mk} \tag{12}$$

where l_m and l_k are the distances from the centroid of the surface $\partial\Omega_{mk}$ to the centroids of the elements m and k, respectively (see Fig. 2). Although this splitting scheme does not guarantee accurate error estimates, it provides us with a systematic method of decomposing $\vec{\rho}_{mk}$. This splitting scheme constitutes only the first part of the complete approach developed by Ohtsubo and Kitamura, since it does not involve any explicit equilibrization of the discontinuities of the interelement boundaries of a particular element. To demonstrate the capabilities of the scheme, we will show numerical results for several test cases in the next section.

At this point, it should be noted that (11) does not properly account for the surfaces at the boundary of the mesh since $\vec{\rho}_m$ is only defined at inter-element boundaries. To find the error in the elements which border the mesh boundary, we must properly incorporate the boundary condition into the equation. For this paper, we consider the Dirichlet and Neumann boundary conditions. For elements on the boundary, (11) is modified to include a surface integral on the mesh boundary and is given by

$$\iiint_{\Omega_m} \frac{1}{j\omega\mu}(\nabla\times\vec{e})\cdot(\nabla\times\vec{\phi}_i) + j\omega\epsilon^*\vec{e}\cdot\vec{\phi}_i + \frac{1}{j\omega\mu\epsilon^*}\nabla\cdot(\epsilon^*\vec{e})(\nabla\cdot\vec{\phi}_i) - (\vec{r}_m\cdot\vec{\phi}_i)\,dv = \iint_{\partial\Omega_m}\vec{\rho}_m\cdot\vec{\phi}_i + \iint_{\partial\Omega_{m0}}\vec{\rho}_{m0}\cdot\vec{\phi}_i\,dS \tag{13}$$

where $\partial\Omega_m$ represents the surfaces of the element which are not on the boundary of the mesh, and $\partial\Omega_{m0}$ represents the surfaces of the element which are. The term $\vec{\rho}_{m0}$ is defined to be

$$\vec{\rho}_{m0} = \hat{n}\times(\vec{H} - \tilde{H}) \tag{14}$$

Neumann boundary conditions are very easy to implement because $\hat{n}\times\vec{H}$ is given on the mesh boundary. For the Dirichlet boundary condition, we set the exact values of $\vec{E}$ at the nodes on the outer boundary to generate the numerical field solution; therefore, there is no error in the numerical solution at the boundary of the mesh. When this condition is enforced on (13), it becomes unnecessary to calculate $\vec{\rho}_{m0}$ on the boundary. It should be noted that for the analysis of the $\vec{H}$-field, one can use the dual form of equation (13) to determine the error. In that case, the perfectly conducting boundaries become Neumann rather than Dirichlet boundary conditions.

The error $\vec{e}$ can now be calculated in an element-by-element manner and added to $\tilde{E}$ to improve the overall accuracy of the numerical solution. It is not necessary to apply this scheme to every element. In many instances, the solution is only important in a small fraction of the elements. For example, in radar cross section (RCS) calculations, we require the field solutions only in the elements which border the outer boundary. Similarly, for scattering matrix calculations, the only field information required is at the input and output planes of the geometry under consideration.

A similar derivation can be performed for the $\vec{H}$ field in the case where the unknowns in the FEM solution are the magnetc fields at the nodes rather than the electric fields.

III. Numerical Efficiency

In order to demonstrate the numerical efficiency of the error reduction approach, one can perform a complexity analysis of asymptotic nature on a cubic problem domain. It is known that for a banded matrix, the elimination (LU-decomposition) of the global FEM matrix requires a number of operations which is proportional to W^2M, where W represents the bandwidth of the matrix, and M denotes the total number of unknowns in the cubic problem domain. Since 8-node, first-order hexahedral elements are employed in the computation of the original FEM solutions, it is deduced that the bandwidth W of the global FEM matrix is given by $W = (3N)^2$ (with 3 unknowns per node). With the total number of unknowns in the cubic problem domain being given by $M = (3N)^3$, where N denotes the average number of nodes along one direction in the cubic problem domain, one finds that the process of elimination of the FEM global matrix requires $81N^4 \times 27N^3 = 2187N^7$ operations. The solution (backsubstitution) process is known to involve a total number of operations which is proportional to WM. Thus, it is seen that the solution process requires $9N^2 \times 27N^3 = 243N^5$ operations, which becomes a small number in comparison to the number of operations in the elimination process for realistic problems with a very large parameter N.

In the element-by-element *a posteriori* calculation of the numerical error, however, 20-node, second-order hexahedral elements are used. Therefore, since the total number of elements is given by $(N-1)^3$ in the cubic problem domain, the total number of operations associated with the matrix solution in the error reduction process (with 3 unknowns per node) is given by $60^3(N-1)^3 = 216,000(N-1)^3$, which is clearly a neglible number (of order N^3) in comparison to the number of operations which are involved in the elimination process of the global matrix (of order N^7) for realistic problems with large N. For problems in which one is mainly interested in the reduction of error in those elements which lie along the surface of the cubic problem domain (such as RCS calculation problems), the total number of operations that is required in the error reduction process is further reduced to $6 \times 60^3(N-1)^2 = 1,296,000(N-1)^2$ (of order N^2). The error reduction scheme is therefore computationally much less expensive than a conventional FEM solution which is applied to the same problem domain.

IV. Numerical Results

To demonstrate the validity of the method, a three-dimensional finite element program has been written. A frontal scheme [9] is used to solve the sparse matrix equation for the fields. In this paper, we present the results of the FEM field calculations and the corresponding error reduction procedures for a propagating TE_{10} mode in three rectangular waveguide geometries: an infinite waveguide, a waveguide terminated by a perfect electric conductor, and one terminated by a perfect magnetic conductor. We also present the results of the error reduction scheme when applied to a boundary value problem (Neumann boundary condition specified) which contains a spherical perfectly conducting object. These simple geometries are chosen because the boundary conditions in all four cases are known. In addition, it is easier to analyze the effectiveness of the method on simpler geometries.

To measure the error reduction, we compare the y components of the original FEM solution ($\tilde{E}_y$) and the improved solution ($\tilde{E}_y + e_y$) to the y component of the exact solution (E_y). The error percentages associated with the original and improved solutions can be found in terms of an energy norm from the equations,

$$ep_1 = \left[\frac{\iiint_\Omega |E_y - \tilde{E}_y|^2\, dv}{\iiint_\Omega |E_y|^2\, dv}\right]^{1/2} \times 100\% \qquad (15)$$

$$ep_2 = \left[\frac{\iiint_\Omega |E_y - \tilde{E}_y - e_y|^2\, dv}{\iiint_\Omega |E_y|^2\, dv}\right]^{1/2} \times 100\% \qquad (16)$$

where ep_1 and ep_2 are the error percentages for the original FEM solution and the improved solution, respectively. For the fourth problem, in which the dual $\vec{H}$-formulation of the error reduction scheme is used, we compare the y and z components of the original FEM solution ($\tilde{H}$) and the improved solution $\tilde{H} + \vec{h}$ to the corresponding components of the exact solution ($\vec{H}$).

A. Infinite Rectangular Waveguide

Let us consider a rectangular waveguide (infinite in z direction) of width 0.6λ (along x direction) and height 0.2667λ (along y direction) where λ is the free space wavelength. The walls of the waveguide are assumed to be perfectly conducting. The problem domain is defined by the walls of the waveguide and two fictitious surfaces located at $z = -1.2\lambda$ and $z = 0$ (referred to as input and output surfaces, respectively). The geometry is shown in Fig. 3.

Because the analytical solution is known for this case, the boundary conditions can easily be found for the problem domain. At the side walls of the waveguide, we can apply the appropriate Dirichlet or Neumann boundary conditions for a TE_{10} mode. At the two fictitious surfaces, the exact Neumann boundary condition is specified.

Four different mesh densities are chosen to test the effectiveness of the *a posteriori* error reduction scheme on the above geometry. The four meshes are made up of 72, 144, 240, and 360 elements. The corresponding number of nodes

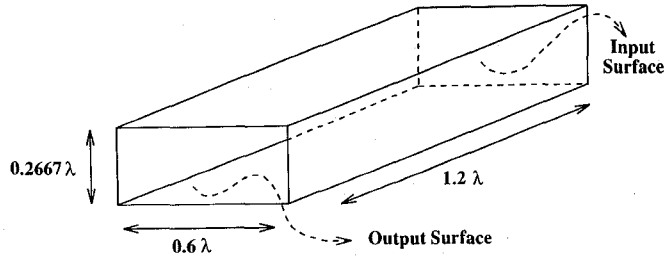

Fig. 3. A 1.2λ section of an infinite rectangular waveguide of width 0.6λ and height 0.2667λ.

TABLE I
A TABULATION OF THE ERROR PERCENTATIONS FOR THE THREE WAVEGUIDE EXAMPLES. CASE 1 IS AN INFINITE WAVEGUIDE; CASE 2 IS A WAVEGUIDE TERMINATED BY A PERFECT ELECTRIC CONDUCTOR; CASE 3 IS A WAVEGUIDE TERMINATED BY A PERFECT MAGNETIC CONDUCTOR

Waveguide Example	Number of Elements	ep_1 (%)	ep_2 (%)
Case 1	72	41.4	25.7
	144	15.4	9.9
	240	8.3	5.3
	360	3.4	2.9
Case 2	72	34.2	31.3
	144	15.0	14.7
	240	8.5	8.6
	360	5.5	5.6
Case 3	72	47.7	28.8
	144	17.6	10.8
	240	9.5	5.8
	360	6.0	3.7

for 8-node hexahedral elements is 150, 274, 432, and 627, while the number of nodes for 20-node hexahedral elements is 505, 941, 1509, and 2209. The 8-node hexahedron mesh is used to compute $\tilde{E}$, and the 20-node hexahedron mesh is used to compute $\vec{e}$ in an element-by-element manner. The error percentages, ep_1 and ep_2 are listed in Table I for all four meshes under Case 1. From the results, it is evident that the scheme produces significant error reduction.

To get a better idea of how the error is distributed along the length of the waveguide, let us define two quantities,

$$E_{diff1} = |E_y - \tilde{E}_y| \tag{17}$$

$$E_{diff2} = |E_y - (\tilde{E}_y + e_y)| \tag{18}$$

In Fig. 4, we plot the normalized quantities E_{diff1}/E^i and E_{diff2}/E^i as a function of z for the 360 element mesh, where E^i denotes the amplitude of the "incident" electric field in the waveguide. The fields are evaluated at a fixed value of x and y, corresponding to the point where E_y is maximum (the center of the waveguide cross section). The solution is discontinuous at the inter-element boundaries because the solution in any single element is decoupled from the other

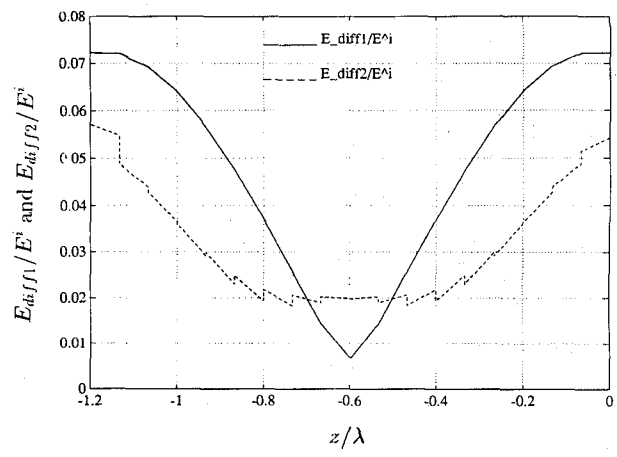

Fig. 4. Plot of E_{diff1}/E^i and E_{diff2}/E^i at the center of the cross section of the waveguide as a function of z for the infinite rectangular waveguide (360 element case).

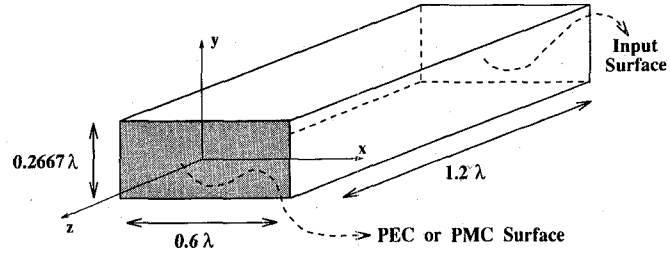

Fig. 5. A 1.2λ section of a semi-infinite rectangular waveguide of width 0.6λ and height 0.2667λ, which is terminated at one end by either a perfect electric conductor (PEC) or perfect magnetic conductor (PMC).

elements. Although we violate the continuity condition, the error has been significantly reduced. The improved solution has less error than the original solution except near the middle of the waveguide, where the original solution has almost zero error. It is also interesting to observe that the error reduction at the input and output surfaces is not as effective. It seems that the strict enforcement of the exact Neumann boundary condition in the error reduction scheme has a negative impact; therefore, it is best not to use the input and output surfaces for any future calculations. Instead, the solutions in the adjacent elements should be used whenever possible to calculate the parameters of interest.

B. Rectangular Waveguide Terminated by a Perfect Electric or Perfect Magnetic Conductor

Let us modify the geometry in the first example by terminating the waveguide with a perfect electric conductor at $z = 0$ (Fig. 5); therefore, a standing wave is set up inside the guide when a TE_{10} mode is incident on the perfect electric conductor. To reflect this change, we must impose the homogeneous Dirichlet boundary condition at $z = 0$. At the input surface, we still apply the exact Neumann boundary condition. In Table I under Case 2, we present the error percentages for this geometry using the four meshes described in the first example. Unlike the previous case, there appears to be very little error reduction when the a posteriori scheme is applied. In fact, the error percentages actually increase.

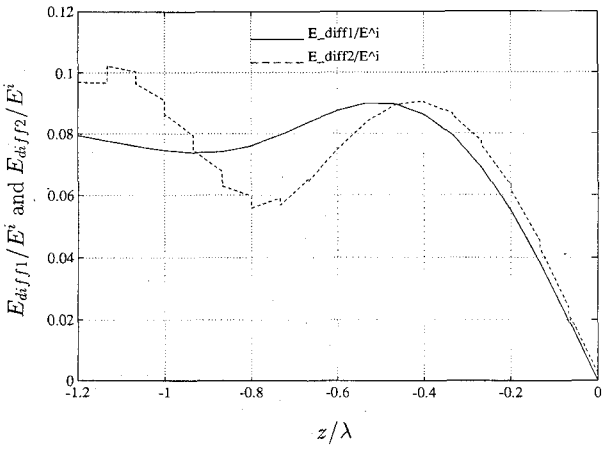

Fig. 6. Plot of E_{diff1}/E^i and E_{diff2}/E^i at the center of the cross section of the waveguide as a function of z for the rectangular waveguide terminated by a perfect electric conductor (360 element case).

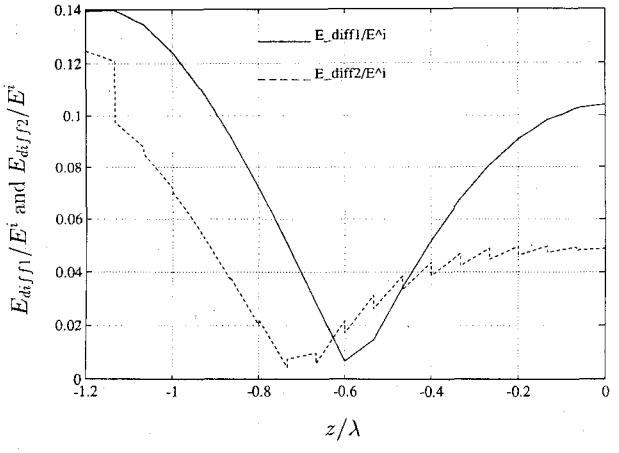

Fig. 7. Plot of E_{diff1}/E^i and E_{diff2}/E^i at the center of the cross section of the waveguide as a function of z for the rectangular waveguide terminated by a perfect magnetic conductor (360 element case).

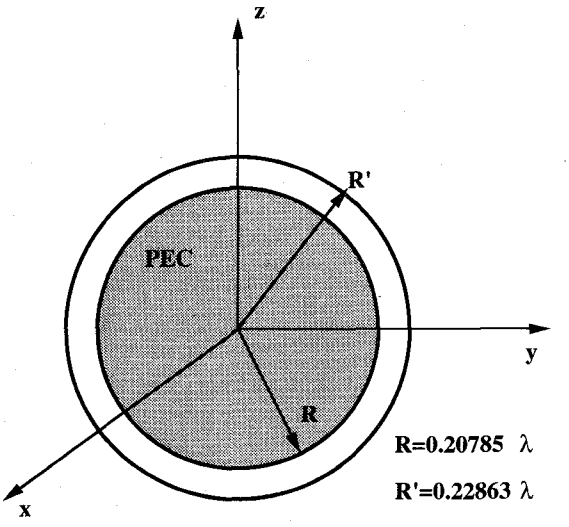

Fig. 8. Geometry of the PEC sphere.

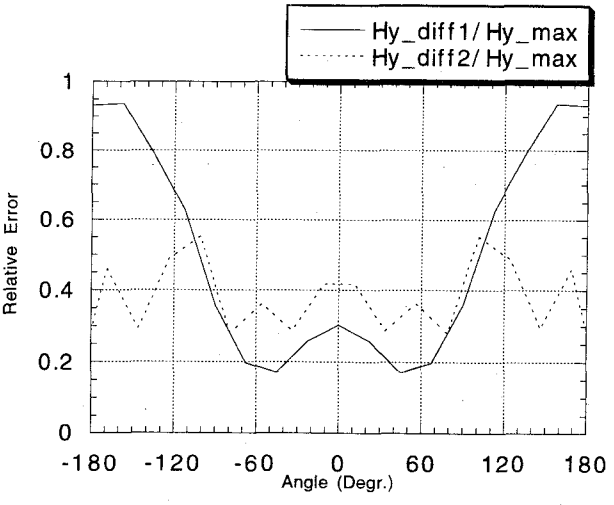

Fig. 9. Plot of Hy_{diff1}/Hy_{max} and Hy_{diff2}/Hy_{max} on the surface of the PEC sphere as a function of angle.

In Fig. 6, we plot E_{diff1}/E^i and E_{diff2}/E^i at the center of the waveguide cross section as a function of z for the 360 element mesh. Again, the plot clearly indicates that there is little or no error reduction throughout the entire mesh. Since the only difference between the first and second examples is the imposition of a Dirichlet boundary condition at the perfect electric conductor, we suspect that the Dirichlet boundary condition may cause the failure in the error reduction scheme. To test this hypothesis, we consider a third geometry in which the perfect electric conductor is replaced by a perfect magnetic conductor. In this instance, a homogeneous Neumann boundary condition is applied at $z = 0$. The error percentages for the four different meshes are shown in Table I under Case 3. We observe that the error reduction for this case is very similar to the first case; therefore, we suggest that Neumann boundary conditions be used whenever possible. For example, the second case can be formulated in terms of the magnetic field, so that all the boundary conditions are of the Neumann type. The Dirichlet boundary condition results in a zero error condition in the original FEM field solution at the boundary in question, which in turn leads to an entirely different distribution of the error along the waveguide. The Neumann boundary condition results in a build-up of the error at that boundary, which implies an error distribution that is more suitable for the application of the error reduction scheme. Also, the Neumann boundary condition can be used for boundary truncation techniques such as the unimoment and bymoment methods [10], [11].

The error distribution at the center of the waveguide crossection as a function of z for the 360 element mesh is shown in Fig. 7. We can see that the error reduction is greater at the perfect magnetic conductor than at the input surface. This observation implies that the homogeneous Neumann boundary condition is more successfully incorporated into the error reduction scheme than the exact Neumann boundary condition. The asymmetric distribution of the quantity E_{diff1}/E^i along the z-direction in this particular numerical example, in contrast to E_{diff1}/E^i in the first numerical example, is a consequence of the fact that the homogeneous and the exact Neumann boundary conditions are placed at opposite ends of the waveguide.

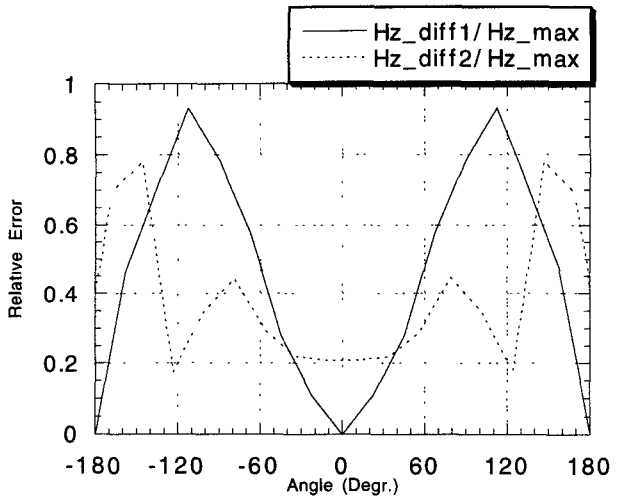

Fig. 10. Plot of Hz_{diff1}/Hz_{max} and Hz_{diff2}/Hz_{max} on the surface of the PEC sphere as a function of angle.

C. Perfectly Conducting Sphere

In the last example, a perfect electric conducting (PEC) sphere (Fig. 8) is illuminated by the fields produced from two scalar potentials which are represented by the spherical vector wave functions $\vec{M}_{11}$ and $\vec{N}_{11}$ as defined by Stratton [12]. There are two layers of elements between the conducting sphere and the outer boundary of the mesh. The total number of elements in the mesh is 192. In order to consider the PEC sphere with Neumann boundary conditions, the $\vec{H}$-fields are specified as the FEM unknowns. The error is given by

$$H_{diff1} = |H - \tilde{H}| \tag{19}$$

$$H_{diff2} = |H - (\tilde{H} + h)| \tag{20}$$

The above two equations are used for both the y and z components of $\vec{H}$. In Figs. 9 and 10, Hy_{diff} and Hz_{diff} are plotted along the surface of the sphere as a function of the angle. The terms Hy_{max} and Hz_{max} represent the maximum values of the exact field on the surface of the PEC sphere. We see that the *a posteriori* solution is more accurate except near the zero degree angle.

V. Summary

An *a posteriori* error reduction scheme for the finite element method has been applied to solve three dimensional electromagnetic boundary value problems. The scheme is based upon the fact that the numerical solution does not satisfy Maxwell's equations exactly, producing a residual error term. Furthermore, some of the tangential fields are discontinuous at inter-element boundaries. These two pieces of information can be used to predict the error in the numerical solution in an element-by-element manner. The predicted error is then used to cancel the error in the numerical solution. The scheme has been tested for three waveguide geometries. From the numerical results, it is evident that there was significant improvement in the solution.

References

[1] I. Babuska, "The selfadaptive approach in the finite element method," in J. R. Whiteman (Ed.), *Mathematics of Finite Elements and Applications.* London: Academic, 1975.

[2] D. W. Kelly, J. P. De S. R. Gago, and O. C. Zienkiewicz, "*A posteriori* error analysis and adaptive processes in the finite element method: part I—error analysis," *Int. J. Num. Methods Eng.*, Vol. 19, pp. 1593–1619, 1983.

[3] J. P. De S. R. Gago, D. W. Kelly, O. C. Zienkiewicz, and I. Babuska, "*A posteriori* error analysis and adaptive processes in the finite element method: part II—adaptive mesh refinement," *Int. J. Num. Methods Eng.*, Vol. 19, pp. 1621–1656, 1983.

[4] O. C. Zienkiewicz and J. Z. Zhu, "A simple error estimator and adaptive procedure for practical engineering analysis," *Int. J. Num. Methods Eng.*, Vol. 24, pp. 337–357, 1987.

[5] J. Z. Zhu and O. C. Zienkiewicz, "Adaptive techniques in the finite element method," *Comm. Applied Numerical Methods*, Vol. 4, pp. 197–204, 1988.

[6] D. W. Kelly, "The self-equlibration of residuals and complementary *a posteriori* error estimates in the finite element method," *Int. J. Num. Methods Eng.*, Vol. 20, pp. 1491–1506, 1984.

[7] H. Ohtsubo and M. Kitamura, "Element by element a posteriori error estimation and improvement of stress solutions for two-dimensional elastic problems," *Int. J. Num. Methods Eng.*, Vol. 29, pp. 223–244, 1990.

[8] K. D. Paulsen and D. R. Lynch, "Elimination of Vector Parasites in Finite Element Maxwell Solutions," *IEEE Trans. Microwave Theory Tech.*, MTT-39, pp. 395–404, Mar. 1991.

[9] B. M. Irons, "A frontal solution program for finite element analysis," *Int. J. Num. Methods Eng.*, Vol. 2, pp. 5–32, 1970.

[10] K. K. Mei, "Unimoment method of solving antenna and scattering problems," *IEEE Trans. Antenn. Propagat.*, AP-22, pp. 760–766, Nov. 1974.

[11] A. C. Cangellaris and R. Lee, "The bymoment method for two-dimensional electromagnetic scattering," *IEEE Trans. Antenn. Propagat.*, AP-38, pp. 1429–1437, Sept. 1990.

[12] J. A. Stratton, *Electromagnetic Theory.* New York: McGraw-Hill, 1941.

Ümit Pekel, received the B.S. and M.S. degrees in electrical engineering in 1985 and 1987, respectively, from the Middle East Technical University, Ankara, Turkey. He received the Ph.D. degree at The Ohio State University in 1993 and is currently working as a postdoctoral research associate at the Electromagnetic Communication Laboratory at the University of Illinois at Urbana-Champaign.

Robert Lee (S'82–M'83–S'85–M'90), for a biography, see page 2301 of the December 1994 issue of this TRANSACTIONS.